Detection of correlated galaxy ellipticities on CFHT data: first evidence for gravitational lensing by large-scale structures.⋆

L. Van Waerbeke[1], Y. Mellier[2,3], T. Erben[4], J.C. Cuillandre[5], F. Bernardeau[6], R. Maoli[2], E. Bertin[2,3], H.J. Mc Cracken[7], O. Le Fèvre[7], B. Fort[2], M. Dantel-Fort[3], B. Jain[8], P. Schneider[4]

[1] Canadian Institut for Theoretical Astrophysics, 60 St Georges Str., Toronto, M5S 3H8 Ontario, Canada.
[2] Institut d'Astrophysique de Paris. 98 bis, boulevard Arago. 75014 Paris, France.
[3] Observatoire de Paris. DEMIRM. 61, avenue de l'Observatoire. 75014 Paris, France.
[4] Max Planck Institut fur Astrophysiks, Karl-Schwarzschild-Str. 1, Postfach 1523, D-85740 Garching, Germany.
[5] Canada-France-Hawaii-Telescope, PO Box 1597, Kamuela, Hawaii 96743, USA
[6] Service de Physique Théorique. C.E. de Saclay. 91191 Gif sur Yvette Cedex, France.
[7] Laboratoire d'Astronomie Spatiale, 13376 Marseille Cedex 12, France
[8] Dept. of Physics, Johns Hopkins University, Baltimore, MD 21218, USA

March 16, 2000

Abstract. We report the detection of a significant (5.5 σ) excess of correlation between galaxy ellipticities at scales ranging from 0.5 to 3.5 arc-minutes. This detection of a gravitational lensing signal by large-scale structure was made using a composite high quality imaging survey of 6300 arcmin^2 obtained at the Canada France Hawaii Telescope (CFHT) with the UH8K and CFH12K panoramic CCD cameras. The amplitude of the excess correlation is 2.4%, in agreement with the theoretical predictions of the lensing effect induced by large-scale structure. We provide a quantitative analysis of systematics which could contribute to the signal and show that the net effect is small and can be corrected for. In particular, we show that the spurious excess of correlation caused by the residual of the anisotropic Point Spread Function (PSF) correction is well below the measured signal. We show that the ellipticity correlation signal behaves as the predictions given by the gravitational lensing theory. The relatively small size of our survey precludes tight constraints on cosmological models, although the data are in agreement with cluster normalized models, and marginally reject cold dark matter models with ($\Omega = 0.3$, $\sigma_8 < 0.6$) or ($\Omega = 1$, $\sigma_8 = 1$). The detection of cosmic shear demonstrates the technical feasibility of using weak lensing surveys to measure dark matter clustering and the potential for cosmological parameter measurements, in particular with upcoming wide field CCD cameras.

Key words: Cosmology: theory, dark matter, gravitational lenses, large-scale structure of the universe

Send offprint requests to: waerbeke@cita.utoronto.ca

⋆ Based on observations obtained at the Canada-France-Hawaii Telescope (CFHT) which is operated by the National Research Council of Canada (NRCC), the Institut des Sciences de l'Univers (INSU) of the Centre National de la Recherche Scientifique (CNRS) and the University of Hawaii (UH)

1. Introduction

The measurement of gravitational weak lensing produced by the cosmic structures (hereafter, the cosmic shear) is the ultimate, albeit most challenging, step toward a direct mapping of the dark matter distribution in our Universe, without regards on the distribution of light emitted by gas and galaxies.

A decade of theoretical and technical studies have shown that the gravitational weak distortion produced by hierarchical distribution of structures along line of sights do contains important clues on the cosmological scenario of structures formation which should be recovered from deep wide field surveys of galaxies (see Mellier 1999, Bartelmann & Schneider (2000) for reviews and references therein). From these studies, we know that, in principle, weak lensing analysis permits to measure the cosmological parameters and the shape of the power spectrum of density fluctuations (Kaiser 1992, Villumsen 1996, Bernardeau et al. 1997, Jain & Seljak 1997, Kaiser 1998, Schneider et al. 1998,

Bartelmann & Schneider 1999). However, they have also revealed that the most challenging issues are technical, because the measurement of extremely weak gravitational distortion has to deal with strong sources of noise and systematics such as the photon noise, the optical distortion of astronomical telescopes and the atmospheric distortion. Therefore, the problem of reliable shape measurement has also received much attention in the last few years (Bonnet & Mellier 1995, Kaiser et al. 1995, Van Waerbeke et al. 1997,
Hoekstra et al. 1998, Kuijken 1999, Rhodes et al. 1999, Kaiser 1999, Bertin 2000).

Despite considerable difficulties in recovering weak lensing signal, the strong cosmological interest of the cosmic shear analysis has motivated many teams to devote huge efforts on imaging surveys in order to measure the galaxy distortion produced by gravitational lensing, either by observing many independent small fields, like the VLT/FORS-I (Maoli et al in preparation), the HST/STIS (Seitz et al 1998), the WHT (Bacon et al in preparation), or by observing few intermediate to large fields, like the CFHT/CFH12K-UH8K (this work), or the SDSS (Annis et al 1998). In this paper we present the results of the analysis based on 2. square degrees obtained during previous independent observing runs at CFHT with mixed I and V colors. This study is part of a our weak lensing survey carried out at CFHT (hereafter the DESCART project[1]) which aims at covering 16 square degrees in four colors with the CFH12K camera. Though the survey is far from completion, data obtained during previous runs have been used jointly to the first observations of the DESCART survey that we did in May 1999 and in November 1999 in order to demonstrate that the technical issues are overcome and to better prepare next observations. This set of data permits to already report on the detection of signal.
In the following, we discuss the technique we used in order to extract the cosmological signal and to measure its amplitude and show that systematic effects are well under control. The paper is organized as follows. Section 2 describes our data sets. Section 3 discusses the details of our PSF correction procedure and Section 4 presents the final results. Section 5 is devoted to the discussion of the systematics residuals and their correction. Section 6 presents a preliminary quantitative comparison of our signal with numerical expectations of cosmological scenarios as derived from ray-tracing simulations. Conclusions are given in Section 7.

2. Description of the data sets

The difficulty to get a wide angle coverage of the sky in good conditions is the reason why there is not yet a clear itize the field of view in order to get the widest angular field as possible. This was done at the expense of homogeneity of the data set but it does not impact at all on our primary goals which is the detection of a weak lensing signal and the test of the control of systematics.
We use in total eight different pointings mixing CFH12K and UH8K data sets (see Table 1). They are spread over five statistically independent areas, each separated by more than 10 degrees. The total field covers about 6300arcmin^2, and contains about 3×10^5 galaxies ($n_g \simeq 30 gal/arcmin^2$). However, the galaxies are weighted as discussed in Section 2.2, and parts of the fields are masked, so the effective number density of galaxies is about half.

All the data were obtained at the CFHT prime focus. We used observations spread over 4 years from 1996 to 1999, with two different cameras: the UH8K (Luppino et al 1994), covering a field of 28×28 square arc minutes with 0.2 arc-second per pixel and the CFHT12K [2] (Cuillandre et al 2000) covering a field of 42×28 square arc-minutes with 0.2 arc-second per pixel as well. Because these observations were initially done for various scientific purposes, they have been done either in I or in V bands. Table 1 summarizes the dataset. The SA57 field was kindly provided by M. Crézé and A. Robin who observed this field for another scientific purpose (star counts and proper motions). The UH8K Abell 1942 data were obtained during discretionary time. The F14 and F02 fields are part of the deep imaging survey of 16 square-degrees in BVRI being conducted at CFHT jointly by several French teams. This survey is designed to satisfy several scientific programs, including the DESCART weak lensing program, the study of galaxy evolution and clustering evolution, clusters and AGN searches, and prepare the spectroscopic sample to be studied for the VLT-VIRMOS deep redshift survey (Le Fèvre et al 1998). CFDF-03 is one of the Canada-France-Deep-Fields (CFDF) studied within the framework of the Canada-France Deep Fields, with data collected with the UH8K (Mc Cracken et al in preparation).
The observations were done as usual, by splitting the total integration time in individual exposures of 10 minutes each, offsetting the telescope by of 7 to 12 arc-seconds after each image acquisition. For the I and the V band data, we got between 7 to 13 different exposures per field. The total exposure times range between 1.75 hours in V to 5 hours in I.
The total observed field covers 2.05 square-degrees, including 0.88 square degree in V and 1.17 square degree in I. However, one CCD of the UH8K and two CCDs initially mounted on the CFH12K of the May 1999 run have strong charge transfer efficiency problems and are not suitable for weak lensing analysis. Therefore, the final area only covers 1.74 square degrees: 0.64 square-degree in V and

[1] http://terapix.iap.fr/Descart/

[2] http://www.cfht.hawaii.edu/Instruments/Imaging/CFH12K

Table 1. List of the fields. Most of the exposures were taken in the I band at CFHT. The total area is 1.7 deg^2, and the 8 fields are uncorrelated.

Target	Name	Camera	Used area	Filter	Exp. time	Period	seeing
F14P1	F1	CFH12K	764 arcmin^2	V	5400 sec.	May 1999	0.9"
F14P2	F2	CFH12K	764 arcmin^2	V	5400 sec.	May 1999	0.9"
F14P3	F3	CFH12K	764 arcmin^2	V	5400 sec.	May 1999	0.9"
CFDF-03	F4	UH8K	669 arcmin^2	I	17000 sec.	Dec. 1996	0.75"
SA57	F5	UH8K	669 arcmin^2	I	12000 sec.	May 1998	0.75"
A1942	F6	UH8K	573 arcmin^2	I	10800 sec.	May 1998	0.75"
F02P1	F7	CFH12K	1050 arcmin^2	I	9360 sec.	Nov. 1999	0.8"
F02P4	F8	CFH12K	1050 arcmin^2	I	7200 sec.	Nov. 1999	0.9"

1.1 square degree in I. As we can see from Table 1 each field has different properties (filter, exposure time, seeing) which makes this first data set somewhat heterogeneous.

The data processing was done at the TERAPIX data center located at IAP which has been created in order to process big images obtained with these panoramic CCD cameras[3]. Its CPU (2 COMPAQ XP1000 with 1.2 Gb RAM memory each equipped with DEC alpha ev6/ev67 processors) and disk space (1.2 Tbytes) facilities permit to handle such a huge amount of data without technical difficulty.

For all, but the CFDF-03 field, the preparation of the detrending frames (master bias, master dark, master flats, superflats, fringing pattern, if any) and the generation of pre-reduced and stacked data were done using the FLIPS pre-reduction package (FITS Large Image Pre-reduction software) implemented at CFHT and in the TERAPIX pipeline (Cuillandre et al in preparation). In total, more than 300 Gbytes of data have been processed for this work.

The CFHT prime focus wide field corrector introduces a large scale geometrical distortion in the field (Cuillandre et al 1996). Re-sampling the data over the angular size of one CCD (14 arc-minutes) cannot be avoided if large angular offsets ($>$ 40 arc-seconds) are used for the dithering pattern (like for the CFDF-03 data). Since we kept the offsets between all individual exposures within a 15 arc-seconds diameter disk, the contribution of the distortion between objects at the top and at the bottom of the CCD between dithered exposures is kept below one tenth of a pixel. With the seeing above 0.7" and a sampling of 0.2"/pixel, the contribution of this effect is totally negligible in our data set. We discuss this point in Section 5, in particular by looking at the sensitivity of the shear components with radial distances which is confirmed to be negligible. Also not correcting this optical distortion results in a slightly different plate scale from the center to the edge of the field (pixels see more sky in the outside field). But this is also of no consequence for our program since we look at independent individual objects covering typically 10 to 20 pixels in diameter.

The stacking of the non-CFDF images has been done independently for each individual CCD (each covering 7×14 arc-minutes). We decided not to create a single large UH8K or CFH12K image per pointing since it is useless for our purpose. It complicates the weak lensing analysis, in particular for the PSF correction, and needs to handle properly the gaps between CCDs which potentially could produce discontinuities in the properties of the field. The drawback is that we restricted ourselves to weak lensing analysis on scale smaller than 7 arc-minutes (that is a radius smaller than 3.5 arc-minutes, as shown in the next figures) but this is not a critical scientific issue since the total field of view is still too small to provide significant signal beyond that angular scale. In the following we then consider each individual CCD as the quantum of the data set.

The co-addition was performed by computing first the offset of each CCD between each individual exposure from the identification of common bright objects (usually 20 objects) spread over one of the CCD arbitrary chosen as a reference frame. Then, for each exposure the offsets in the x- and y- directions are computed using the detection algorithm of the SExtractor package (Bertin & Arnouts 1996) which provides a typical accuracy better than one tenth of a pixel for bright objects. The internal accuracy of this technique is given by the rms fluctuations of the offsets of each reference object. Because our offsets were small the procedure works very well and provides quickly a stable solution. We usually reach an accuracy over the CCDs of 0.25 pixels rms (0.05 arc-second) in both directions for offsets of about 10 arc-seconds (50 pixels). Once the offsets are known the individual CCDs are stacked using a bilinear interpolation and by oversampling each pixel by a factor of 5 in both x- and y- directions (corresponding to the rms accuracy of the offsets). The images are then re-binned 1×1 and finally a clipped median procedure is used for the addition. The procedure requires CPU and disk space but works very well, provided the shift between exposure remains small. We then end up with a final set of stacked CCDs which are ready for weak lensing analysis.

[3] http://terapix.iap.fr/

processed independently using a method which is fully described elsewhere (McCracken et al 2000, in preparation). Briefly, it uses astrometric sources present in the field to derive a world coordinate system (WCS; in this work we use a gnomic projection with higher order terms). This mapping is then used to combine the eight CCD frames to produce a single image in which a uniform pixel scale is restored across the field. Subsequent pointings are registered to this initial WCS by using a large number of sources distributed over the eight CCDs to correct for telescope flexure and atmospheric refraction. For each pointing the registration accuracy is $\sim 0.05''$ rms over the entire field. The final twelve projected images are combined using a clipped median, which, although sub-optimal in S/N terms, provides the best rejection for cosmic rays and other transient events for small numbers of input images.

3. Galaxy shape analysis

The galaxies have been processed using the IMCAT software generously made available by Nick Kaiser [4]. Some of the process steps have been modified in order to comply with our specific needs. These modifications are described in this Section.

The object detection, centroid, size and magnitude measurements are done using SExtractor (Bertin & Arnouts 1996 [5]) which is optimized for the detection of galaxies. We replace the parameter r_g (physical size of an object), calculated in the IMCAT peak finder algorithm by the half-light-radius of SExtractor (which is very similar to r_h measured in IMCAT). Before going into the details of our shape analysis, we first shortly review how IMCAT measures shapes and corrects for the stellar ellipticities. Technical details and proofs can be found in Kaiser et al. 1995 (hereafter KSB), Hoekstra et al. 1998 and Bartelmann & Schneider (2000).

3.1. PSF correction: the principle

KSB demonstrates how a gravitational shear and a PSF anisotropy affects the shape of a galaxy. Their derivation takes into account first order effects in order to propose a correction scheme of the image degradation produced by the instrument and the atmosphere. The correction applies on the second moments of each galaxy as it is measured from the ellipticity of their brightness distribution. The ellipticity can be directly linked to the shear and the star anisotropy. The raw ellipticity $\mathbf{e}$ of an object is the quantity measured from the second moments I_{ij} of the surface brightness $f(\boldsymbol{\theta})$:

$$\mathbf{e} = \left(\frac{I_{11}-I_{22}}{Tr(I)}; \frac{2I_{12}}{Tr(I)}\right), \quad I_{ij} = \int \mathrm{d}^2\theta W(\theta)\theta_i\theta_j f(\boldsymbol{\theta}). \quad (1)$$

[4] http://www.ifa.hawaii.edu/~kaiser/

[5] see also ftp://geveor.iap.fr/pub/sextractor/

photon noise which dominates the light distribution of the objects at large radius. In presence of a shear γ_β and a PSF anisotropy p_β, the raw ellipticity is sheared and smeared, and modified by the quantity $\delta\mathbf{e}$:

$$\delta e_\alpha = P^{sh}_{\alpha\beta}\gamma_\beta + P^{sm}_{\alpha\beta}p_\beta. \quad (2)$$

The sheared and smeared polarization tensors $P^{sh}_{\alpha\beta}$ and $P^{sm}_{\alpha\beta}$ are measured from the data, and the stellar ellipticity $\mathbf{p}$, also measured from the data, is given by the raw stellar ellipticity $\mathbf{e}^\star$:

$$p_\alpha = \frac{e^\star_\alpha}{P^{sm}_{\alpha\alpha}}. \quad (3)$$

Using Eq(2) and Eq(3) we can therefore correct for the stellar anisotropy, and obtain an unbiased estimate of the orientation of the shear γ_β. To get the right amplitude of the shear, a piece is still missing: the isotropic correction, caused by the filter $W(\theta)$ and the isotropic part of the PSF, which tend to circularize the objects. Luppino & Kaiser 1997 absorbed this isotropic correction by replacing of the shear polarization P^{sh} in Eq(2) (which is an exact derivation in case of Gaussian PSF) by the preseeing shear polarisability P^γ:

$$P^\gamma = P^{sh} - \frac{P^{sh}_\star}{P^{sm}_\star}P^{sm}. \quad (4)$$

This factor 'rescales' the galaxy ellipticity to its true value, once the stellar anisotropy has been removed. The residual anisotropy left afterwards is the cosmic shear γ_β, therefore the observed ellipticity can be written as the sum of a 'source' ellipticity, a gravitational shear $\boldsymbol{\gamma}$ term and a stellar anisotropy contribution:

$$\mathbf{e}^{obs} = \mathbf{e}^{source} + P_\gamma\boldsymbol{\gamma} + P^{sm}\mathbf{p}. \quad (5)$$

There is no reason that $\mathbf{e}^{source}$ should be the *true* source ellipticity $\mathbf{e}^{true}$, as demonstrated by Bartelmann & Schneider (2000). The only thing we know about $\mathbf{e}^{source}$ is that $\langle\mathbf{e}^{true}\rangle = 0$ implies $\langle\mathbf{e}^{source}\rangle = 0$ since all the anisotropy contribution (shear and stellar) has been sorted out. Therefore Eq(5) provides an unbiased estimate of the shear $\boldsymbol{\gamma}$ as long as the intrinsic ellipticity of the galaxies are uncorrelated (from which $\langle\mathbf{e}^{true}\rangle = 0$ is a consequence). The estimate of the shear is simply given by

$$\gamma = P_\gamma^{-1}\cdot(\mathbf{e}^{obs} - P^{sm}\mathbf{p}) \quad (6)$$

The quantities P^γ, P^{sm} and $\mathbf{p}$ can be calculated for each object with IMCAT. The shear estimate per galaxy (Eq(6)) is done using the matrices of the different polarization tensors, and not their traces (which corresponds to a scalar correction) as we usually see in the literature. Although the difference between tensor and scalar correction is small (because P_γ is nearly proportional to the identity matrix), we show elsewhere, in a comprehensive simulation paper (Erben et al. 2000), that the tensor correction gives the better results.

The process of galaxy detection and shape correction can be done automatically, once we have a sample of stars representative of the PSF. However, in practice the stars selection need much attention and cannot be automated because of contaminations. Stars are eventually so close to a bright neighbor (for instance a small galaxy exactly aligned with it) that their shape parameters are strongly affected. Therefore we adopted a slow but well-controlled manual star selection process: on each CCD, the stars are first selected in the stellar branch of the $r_g - mag$ diagram in order to be certain to eliminate saturated and very faint stars. We then perform a 3σ clipping on the *corrected* star ellipticities, which removes most of the stars whose shape is affected by bright neighbors. It is worth noticing that the σ clipping should be done on the corrected ellipticities and not on the raw ellipticities, since only the corrected ellipticities are supposed to be all centered around zero anisotropy. The stars outliers which survived the σ clipping are checked by eye individually to make sure that no weird systematic are present.
During this procedure, we also manually mask the regions of the CCD which could potentially produce artificial signal. This includes for example the areas with very strong gradient of the sky background, like around bright stars or bright/extended galaxies, but also spikes produced along the diffraction image of the spider supporting the secondary mirror, columns containing light from saturated stars, CCD columns with bad charge transfer efficiency, residuals from transients events like asteroids which cross the CCD during the exposure and finally all the boundaries of each CCD. At the end, we are left with a raw galaxy catalogue and a star catalogue free of spurious objects, and each CCD chip has been checked individually. This masking process removes about 15% of the CCD area and the selection itself leaves about 30 to 100 usable stars per CCD.

The most difficult step in the PSF correction is Eq.(6) where the inverse of a noisy matrix P^γ is involved. If we do not pay attention to this problem, we obtain corrected ellipticities which can be very large and/or negative, then we have to apply severe cuts on the final catalogue to remove aberrant corrections, and many objects are lost. A natural way to solve the problem is to smooth the matrix P^γ before it is inverted. In principle P^γ should be smoothed in the parameter space defining the objects, which can be as large as we want; for example P^γ might depends on the magnitude, the ellipticity, the profile, the size, etc... In practice, it is common to smooth P^γ according to the magnitude and the size (see for instance Kaiser et al. 1998, Hoekstra et al. 1998). We found un-practical to smooth the data on a regular grid, and instead we calculate a smoothed P^γ for each galaxy from its nearest neighbors in the objects parameter space (this has the advantage to find locally the optimal mesh size for a smoothing does not lead to significant improvement in the correction, therefore we keep the magnitude and the size r_h to be the main functional dependencies of P^γ.

A smoothed P^γ does not eliminate all abnormal ellipticities, and the further step is to weight the galaxies according to the noise level of the ellipticity correction. Again, this can be done in the gridded magnitude/size parameter space where each cell contains a fixed number of objects (the nearest neighbors method). We then calculate the variance σ_ϵ^2 of the ellipticity of those galaxies, which gives an indication of the dispersion on ellipticities of the objects in the cell: larger σ_ϵ^2, larger the noise. We then calculate a *weight* w for each galaxy, which is directly given by σ_ϵ^2:

$$w = \begin{cases} \exp(-5(\sigma_\epsilon - \alpha)^2) & \text{if } \sigma_\epsilon < 1 \\ \dfrac{1}{\sigma_\epsilon^2}\exp(-5(1-\alpha)^2) & \text{if } \sigma_\epsilon > 1 \end{cases}, \tag{7}$$

where α is a free parameter, which is chosen to be the maximum of the ellipticity distribution of the galaxies. Eq.(7) might seems arbitrary compared to the usual $1/\sigma_\epsilon^2$ weighting, but we found that the inverse square weighting tends to overweight low-noise objects (because of the divergence for vanishing σ_ϵ^2), and we prefer to suppress this divergence by the exponential cut-off as defined in Eq.(7)[6].

The weighting function prevents the use of an arbitrary and violent cut which we should use otherwise in order to remove the bad objects. However, we found in our simulations (Erben et al. 2000) that we should remove objects smaller than the seeing size, since they carry very poor lensing information, and the PSF convolution is likely to dominate the shear amplitude. Our final catalogue contains about 191000 galaxies, which of them 23000 are masked. It is a galaxy number density of about $n \simeq 26$ gal/arcmin^2, although the effective number density when the weighting is considered should be much less. We find $\alpha = 0.5$, which corresponds to the ellipticity variance of the whole catalogue.

4. Measured signal

The quantity directly accessible from the galaxy shapes and directly related to the cosmology is the variance of the shear $\langle\gamma^2\rangle$. An analytical estimate of it using a simplified cosmological model (power law power spectrum, sources at a single redshift plane, leading order of the perturbation theory, and no cosmological constant) gives (Kaiser 1992, Villumsen 1996, Bernardeau et al. 1997, Jain & Seljak 1997):

$$\langle\gamma^2\rangle^{1/2} \simeq 0.01\sigma_8\Omega_0^{0.75}z_s^{0.75}\left(\frac{\theta}{1\text{arcmin}}\right)^{-\left(\frac{n+2}{2}\right)}, \tag{8}$$

[6] Note that the use of a different weighting scheme like $w \propto 1/(\alpha^2 + \sigma_\epsilon^2)$ has almost no effect on the detection.

malization and z_s the redshift of the sources. θ is the top-hat smoothing filter radius. The expected effect is at the percent level, but at small scale the non-linear dynamic is expected to increase the signal by a factor of a few (Jain & Seljak 1997). Nevertheless Eq.(8) has the advantage to tell us clearly the cosmological dependence of the variance of the shear.

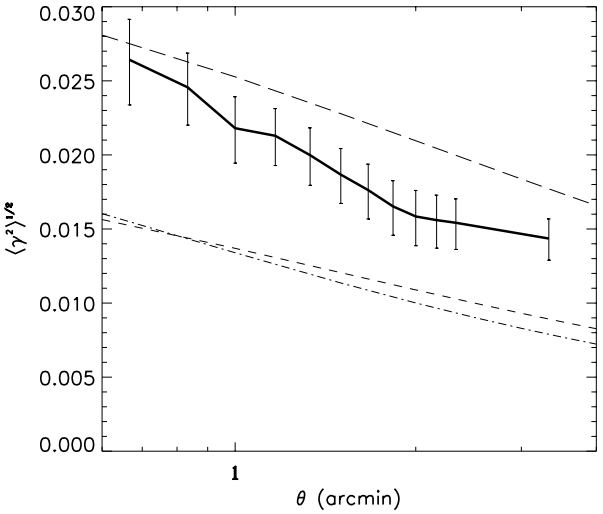

Fig. 1. Square-root of the variance of the measured shear as a function of the radius of the top-hat window (solid line). The maximum angular scale, 3.5 arc-minutes radius, is fixed by the maximum angular scale defined by individual CCDs (7'). Error bars are computed over 1000 random realizations of the galaxy catalogue. The other lines are theoretical predictions of the same quantity for different cosmological models in the non-linear regime (using the fitting formula in Peacock & Dodds 1996): the long-dashed line corresponds to $(\Omega = 1, \Lambda = 0, \sigma_8 = 0.6)$, the dashed line to $(\Omega = 0.3, \Lambda = 0, \sigma_8 = 0.6)$, and the dot-dashed line to $(\Omega = 0.3, \Lambda = 0.7, \sigma_8 = 0.6)$.

¿From the unweighted galaxy ellipticities e_α, an estimate of $\gamma^2(\boldsymbol{\theta}_i)$ at the position $\boldsymbol{\theta}_i$ is given by:

$$E[\gamma^2(\boldsymbol{\theta}_i)] = \sum_{\alpha=1,2} \left(\frac{1}{N} \sum_{k=1}^{N} e_\alpha(\theta_k) \right)^2 . \quad (9)$$

The inner summation is performed over the N galaxies located inside the smoothing window centered on $\boldsymbol{\theta}_i$, and the outer summation over the ellipticity components. The ensemble average of Eq.(9) is

$$\langle E[\gamma^2(\boldsymbol{\theta}_i)] \rangle = \frac{\sigma_\epsilon^2}{N} + \langle \gamma^2 \rangle. \quad (10)$$

The term σ_ϵ^2/N can be easily removed using a random realization of the galaxy catalogue: each position angle of is calculated again. This randomization allows us to determine σ_ϵ^2/N and the error bars associated with the noise due to the intrinsic ellipticity distribution. In practice at least 1000 random realizations are required in order to have a precise estimate of the error bars. Note that it is strictly equivalent to use an estimator where the diagonal terms are removed in the sum (9), which suppress automatically the σ_ϵ^2/N bias.

When we take into account the weighting scheme for each galaxy, the estimator Eq.(9) has to be modified accordingly, and it writes:

$$E[\gamma^2(\boldsymbol{\theta}_i)] = \sum_{\alpha=1,2} \left(\frac{\sum_{k=1}^{N} w(\theta_k) e_\alpha(\theta_k)}{\sum_{k=1}^{N} w(\theta_k)} \right)^2 , \quad (11)$$

where w is the weight as defined in Eq.(7). The variance of the shear is not only the easiest quantity to measure, but it is also fairly weakly sensitive to the systematics provided that they are smaller than the signal. The reason is that any spurious alignment of the galaxies, in addition to the gravitational effect, adds quadratically to the signal and not linearly:

$$\langle \gamma_{mes}^2 \rangle = \langle \gamma_{true}^2 \rangle + \langle \gamma_{bias}^2 \rangle. \quad (12)$$

Therefore, a systematic of say 1% for a signal of 3% only contributes to $\sim 5\%$ in $\langle \gamma^2 \rangle^{1/2}$. We investigate in detail in the next Sections the term $\langle \gamma_{bias}^2 \rangle$ and show that it has a negligible contribution.

We first give our final result of the shear variance measurement on the data sets described in Section 2. The variance $\langle \gamma_{mes}^2 \rangle$ is measured on a grid of density 10×20 pixels for each 2000×4000 CCD. Figure 1 shows $\langle \gamma_{mes}^2 \rangle^{1/2}$ (thick line) with error bars obtained from 1000 random realizations. The three other thin lines correspond to theoretical predictions obtained from an exact numerical computation for three different cosmological models, in the non-linear regime. We assumed a normalized broad source redshift distribution given by

$$n(z_s) = \frac{\beta}{z_0 \Gamma\left(\frac{1+\alpha}{\beta}\right)} \left(\frac{z_s}{z_0}\right)^\alpha \exp\left(-\left(\frac{z_s}{z_0}\right)^\beta\right), \quad (13)$$

with the parameters $(z_0, \alpha, \beta) = (0.9, 2, 1.5)$ are supposed to match roughly the redshift distribution in our data sets [7]. The variance of the shear $\langle \gamma^2 \rangle$ is computed via the formula (see Schneider et al. 1998 for the notations):

$$\langle \gamma^2 \rangle = 2\pi \int_0^\infty k \mathrm{d}k P_\kappa(k) I_{TH}^2(k\theta), \quad (14)$$

[7] with a source redshift distribution which peaks at 0.9

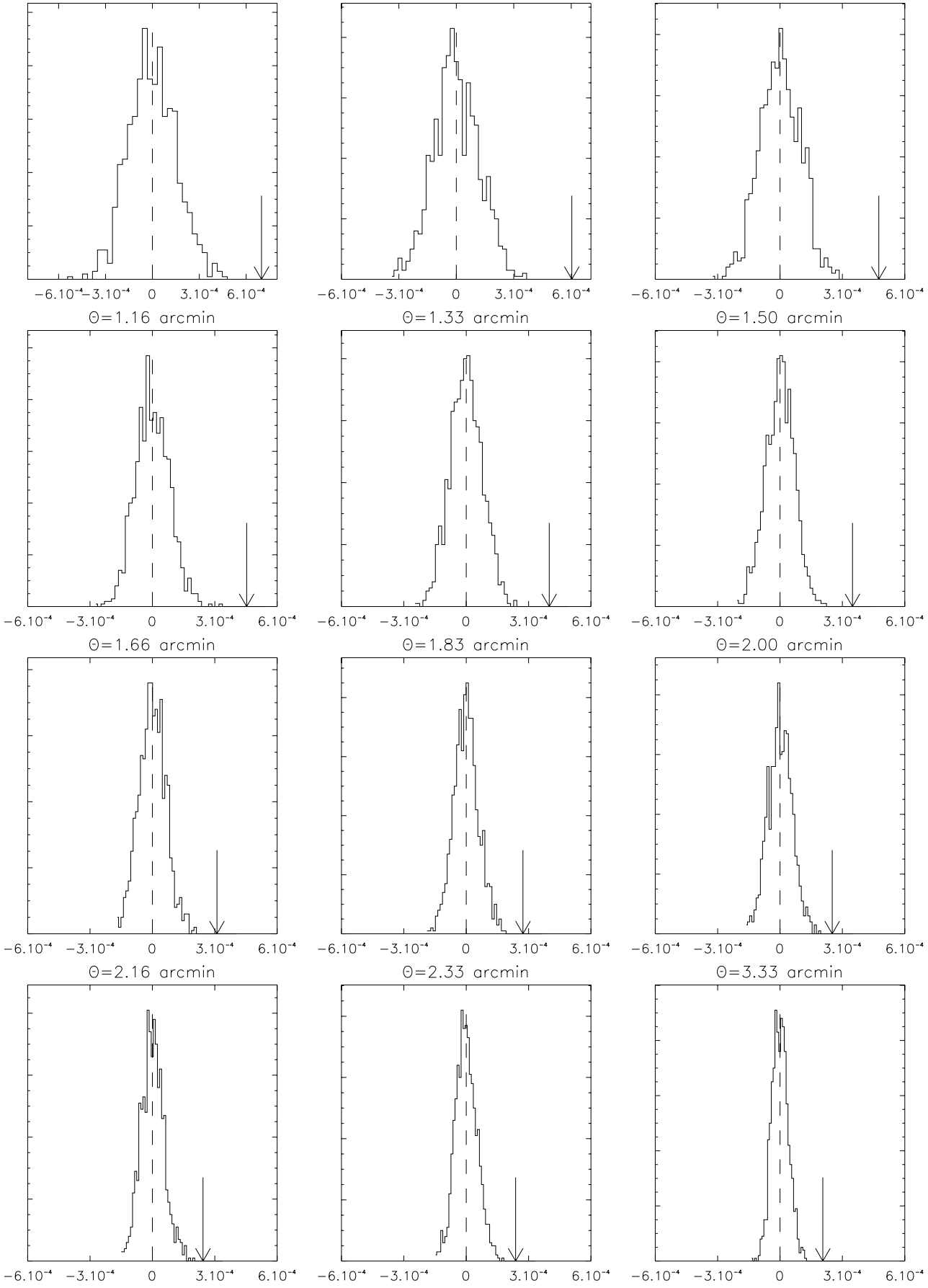

Fig. 2. For different smoothing sizes (indicated at the top of each panel), the value of the measured signal (given by the arrow) compared to the signal measured in the randomized catalogues (histograms). This Figure shows how far is the signal from a pure random orientation of the galaxies. Note that the distribution of $\langle\gamma^2\rangle^{1/2}$ is not Gaussian.

function, and $P_\kappa(k)$ is the convergence power spectrum, which depends on the projected 3-dimensional mass power spectrum $P_{3D}(k)$:

$$P_\kappa(k) = \frac{9}{4}\Omega_0^2 \int_0^{w_H} \frac{\mathrm{d}w}{a^2(w)} P_{3D}\left(\frac{k}{f_K(w)}; w\right) \times \int_w^{w_H} \mathrm{d}w' n(w') \frac{f_K(w'-w)}{f_K(w')}. \quad (15)$$

$f_K(w)$ is the comoving angular diameter distance out to a distance w (and w_H is the horizon distance), and $n(w(z))$ is the redshift distribution of the sources. The non linear mass power spectrum $P_{3D}(k)$ is calculated using a fitting formula (Peacock & Dodds 1996).

We see on Figure 1 that the measured signal is consistent with the theoretical prediction, both in amplitude and in shape. In order to have a better idea of how is significant the signal we can compare for each smoothing scale the histogram of the shear variance in the randomized samples and the measured signal. This is what is shown on Figure 2, for all the smoothing scales shown in Figure 1. The signal is up to 5.5σ significant.

5. Analysis of the systematics

Let us now detail how we end up with a result such as shown in Figure 1. In particular the important issue is to check that the known systematics cannot be responsible for this signal. In the following we discuss three types of systematics:

- The intrinsic alignment of galaxies which could exists in addition to the lensing effect. We assume such alignments do not exist, but unfortunately the overlapping isophotes of close galaxies can produce them. We could in principle remove this effect by choosing a window function small compared to the galaxy distance in the pair, such that close galaxies do not influence the second moment calculation of themselves. However it is difficult to achieve in practice.
- The most known systematics is the PSF anisotropy caused by the telescope tracking errors, the optical distortion, or any imaginable source of anisotropy of the star ellipticity. We have to be sure that the PSF correction outlined in Section 2.2 removes any correlation between galaxy and star ellipticity.
- The spurious alignment of the galaxies along the CCD frame lines/columns. We cannot reject this possibility since charge transfer along the readout directions is done by moving the charges from a pixel to the next pixel and so forth, with an transfer efficiency of 0.99998. This effect could spread the charges of the bright objects (very bright and saturated stars produce this kind of alignment, but they have been removed during the masking procedure). Therefore we out direction.

5.1. Systematics due to overlapping isophotes

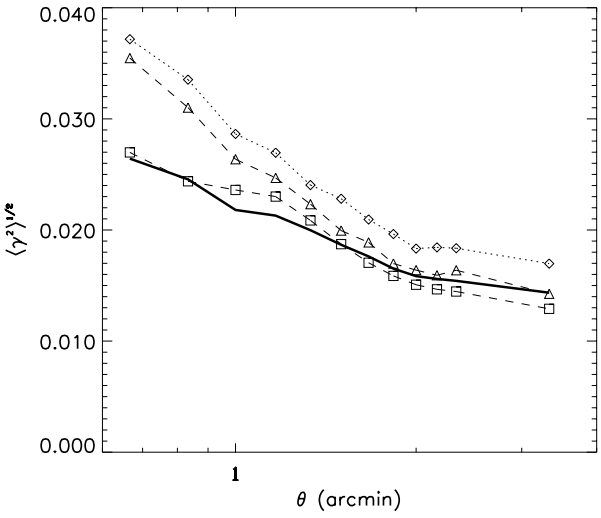

Fig. 3. The thick solid line shows the signal as plotted on Figure 1. It was obtained with a catalogue of galaxies where galaxies closer than 10 pixels were rejected. The three other curves show the same signal measured with different rejection criteria: the diamond-dotted line is for no rejection at all, the triangle-dashed line for galaxies closer than 5 pixels rejected and the square-dashed line for galaxies closer than 20 pixels rejected. This figure illustrates that the overlapping isophotes of close galaxies tends to overestimate the shear.

Let us consider the first point in the above list of systematics. In order to study the effect of close galaxy pairs, we measured the signal by removing close pairs with a varying cut-off of the distance of the galaxies. Figure 3 shows the signal measured when successively pairs closer than $d = 0$ (no pair rejection), 5, 10 and 20 pixels have been rejected. The cases $d = 0$ and $d = 5$ show an excess of power at small scale compared to $d = 10$ and $d = 20$ (the later give the same signal). Therefore we assume that for $d > 10$ we have suppressed the overlapping isophote problem, and in the following we keep the $d = 10$ distance cut-off, which gives us a total of ~ 168000 galaxies for the whole data sets, as already indicated at the end of Section 3.2. By removing close pairs of galaxies, we also remove the effect of potential alignment of group's galaxies caused by tidal forces.

5.2. Systematics due to the anisotropic PSF correction

We next study the second point concerning the residual of the PSF correction. Figures 10 to 15 show the uncorrected and the corrected ellipticity of the stars on the CCD

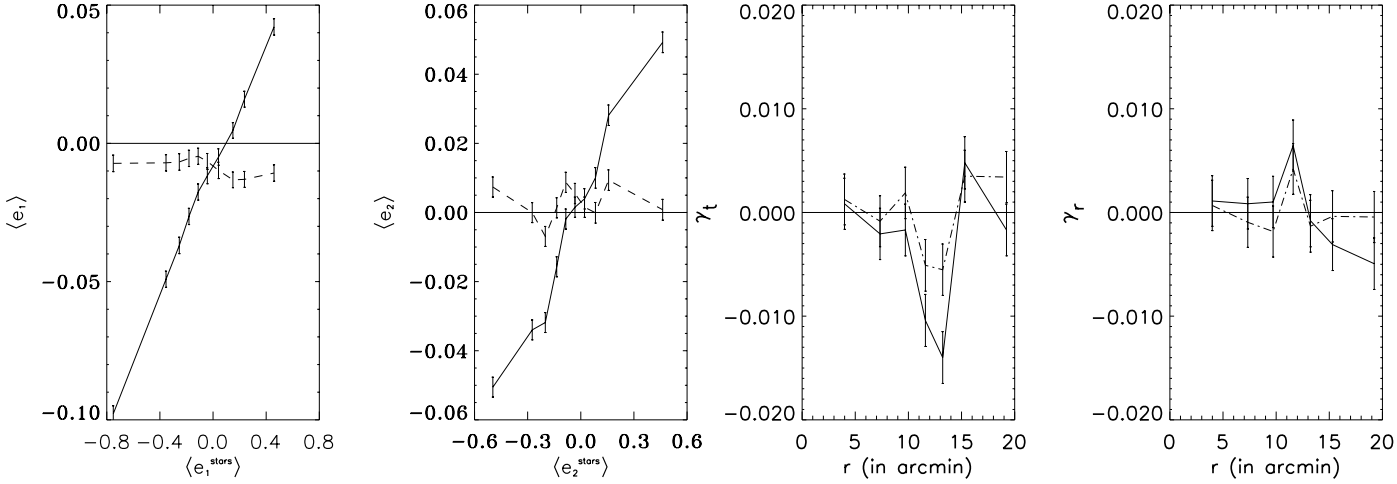

Fig. 4. Average galaxy ellipticity $\langle e_\alpha \rangle$ versus the average star ellipticity $\langle e^\star_\alpha \rangle$ for both components $\alpha = 1, 2$. The dashed lines are obtained from the fully corrected galaxy ellipticities, as given by Eq.(5). The solid lines are obtained from the corrected galaxy ellipticities without the anisotropy correction term $P^{\rm sm}\mathbf{p}$ of Eq.(5). Each ellipticity bin contains about $N = 16000$ galaxies, and the error bars are calculated assuming Gaussian errors $\propto N$. Except a constant tiny bias along the e_1 direction, the corrected galaxies are uncorrelated to the star ellipticity, which demonstrate that the PSF correction method works well.

Fig. 5. Average tangential galaxy ellipticity $\langle \gamma_t \rangle$ and radial galaxy ellipticity $\langle \gamma_r \rangle$ versus the distance from the optical center r. As for Figure 4, the dashed lines are obtained from the fully corrected galaxy ellipticities, as given by Eq.(5), and the solid lines are obtained from the corrected galaxy ellipticities where the anisotropy correction term $P^{\rm sm}\mathbf{p}$ has been removed from Eq.(5). Each ellipticity bin contains about $N = 24000$ galaxies, and the error bars are calculated assuming Gaussian errors $\propto N$. The absence of a significant amplitude between the dashed and the solid lines show that the optical distortion effect is a negligible contribution to the PSF anisotropy.

frames. Using the same camera at different time, we clearly see that the PSF structure can vary a lot in both amplitude and orientation, and that it is not dominated by the optical distortion (as we can see from the location of the optical center, given by the dashed cross). Individual CCD's are $2K \times 4K$ chips, which explains the discontinuities in the stellar ellipticity fields. The measured star ellipticity can be as large as 15%, but the anisotropy of the kernel g of the PSF (see KSB for a definition) can be much larger. The later is given by the quantity $\mathbf{p}$ in Eq.(5), and it is our measure of the ellipticity of a star $\mathbf{e}^{\rm stars}$.

Next, let us sort the galaxies according to the increasing stellar ellipticity, and bin the galaxy catalogue such that each bin contains about few ten thousand galaxies. We then measure, for each bin, two different averages of galaxy ellipticity $\langle e_\alpha \rangle$: one is given by Eq.(5) and the other by Eq.(5) without the anisotropy correction $P^{sm}\mathbf{p}$. The former should be uncorrelated with the star ellipticity if the PSF correction is correct, and we call $\langle e_\alpha \rangle$ such an average; and the later should be strongly correlated with the star ellipticity, and we call it $\langle e^{\rm ani}_\alpha \rangle$. Since the galaxies are binned according to the stellar ellipticity, galaxies of a given bin are taken from everywhere in the survey, therefore the cosmic shear signal should vanish, and the remaining possible non vanishing value for $\langle e_1 \rangle$ and $\langle e_2 \rangle$ should be attributed to a residual of star anisotropy. Figure 4 shows $\langle e_1 \rangle$ and $\langle e_2 \rangle$ (dashed lines) and $\langle e^{\rm ani}_1 \rangle$ and $\langle e^{\rm ani}_2 \rangle$ (solid lines) versus respectively $\langle e^{\rm stars}_1 \rangle$ and $\langle e^{\rm stars}_2 \rangle$. The solid lines exhibit a direct correlation between the galaxy and the star ellipticities, showing that the PSF anisotropy does indeed induce a strong spurious anisotropy in the galaxy shapes of a few percents. However, the dashed lines show that the corrected galaxy ellipticities are no longer correlated with the star ellipticity, the average $\langle e_1 \rangle$ fluctuates around -1%, while $\langle e_2 \rangle$ is consistent with zero. This figure shows the remarkable accuracy of the PSF correction method given in KSB. Error bars in these plots are calculated assuming Gaussian errors for the galaxies in a given bin. The significant offset of $\langle e_1 \rangle$ of 1% might be interpreted as systematic induced by the CCD, as we will see in the next Section, and can be easily corrected for.

Figure 5 shows the same kind of analysis, but instead of sorting the galaxies according to the star ellipticity amplitude, galaxies are now sorted according to the distance r from the optical center. The average quantities we measure are no longer $\langle e_1 \rangle$ and $\langle e_2 \rangle$ versus $\langle e^{\rm stars}_1 \rangle$ and $\langle e^{\rm stars}_2 \rangle$, but the tangential and the radial ellipticity $\langle e_t \rangle$ and $\langle e_r \rangle$ versus r. This new average is powerful to extract any systematic associated with the optical distortion. Figure 5 shows that the systematics caused by the optical distortion is a negligible part of the anisotropy of the PSF, as

anisotropy does obviously not follow the optical distortion pattern).

5.3. Systematics due to the CCD frames

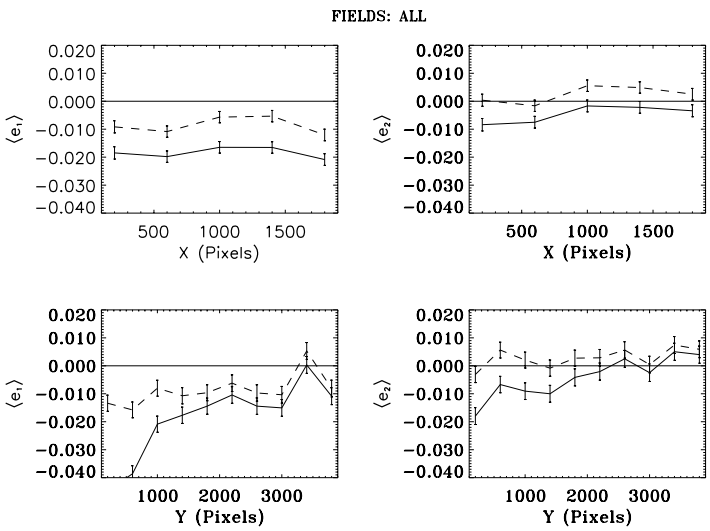

Fig. 6. Average galaxy ellipticity $\langle e_\alpha \rangle$ versus the X and Y location on the CCDs. As for Figure 4, the dashed lines are obtained from the fully corrected galaxy ellipticities, as given by Eq.(5), and the solid lines are obtained from the corrected galaxy ellipticities where the anisotropy correction term $P^{\rm sm}\mathbf{p}$ has been removed from Eq.(5). The systematic negative mean value of $\langle e_1 \rangle$ along lines or columns of the CCD (the two left panels) show that the galaxies are preferentially aligned with the columns of the CCD in the whole survey. A positive systematic value for $\langle e_2 \rangle$ (the two right panels) is is also visible, although much less significant.

Using the same method of the previous Section, we can also investigate the systematics associated with the CCD line/columns orientations. Here, instead of sorting the galaxies according to the star ellipticity or the distance from the optical center, the galaxies are sorted according to their X or Y location on each CCD frame. By averaging the galaxy ellipticities $\langle e_1 \rangle$ and $\langle e_2 \rangle$ in either X or Y bins, we also suppress the cosmic shear signal and keep only the systematics associated with the CCD frame. Figure 6 shows $\langle e_1 \rangle$ and $\langle e_2 \rangle$ (dashed lines) and $\langle e_1 \rangle$ and $\langle e_2 \rangle$ (solid lines) versus $\langle X \rangle$ and $\langle Y \rangle$. The plots from the top-left to bottom-right correspond respectively to $\langle e_1 \rangle$ versus $\langle X \rangle$, $\langle e_2 \rangle$ versus $\langle X \rangle$, $\langle e_1 \rangle$ versus $\langle Y \rangle$, and $\langle e_2 \rangle$ versus $\langle Y \rangle$. We see that $\langle e_1 \rangle$ is systematically negative by an amount of $\sim -1\%$ for both X and Y binnings, while $\langle e_2 \rangle$ does not show any significant deviation from zero. This result is fully consistent with the dashed lines on Figure 4 which demonstrate that the -1% systematic is probably a constant systematic which affects all the galaxies in the same direction. The origin of this constant shift is still not clear, it might eventually be produced during the readout process, since a negative $\langle e_1 \rangle$ corresponds to an anisotropy along columns of the CCDs.

5.4. Test of the systematics residuals

The correction of the constant shift of -1% along $\langle e_1 \rangle$ has been applied to the galaxy catalogue from the beginning. It ensures that there is no more significant residual systematics (either star anisotropy or optical distortion or CCD frame), and it demonstrates that the average level of residual systematics is much below the signal. However, it is not yet enough to ensure that they do not contribute to the observed signal, since it might be that the residual systematics strongly fluctuates around their average value, producing a significant contribution to the variance of the shear. This would be visible for example if, by reducing the number of galaxies in the bins, the averaged galaxy ellipticities would oscillates with a variance of around 3%. We checked that by reducing the number of galaxies in the bins to a number comparable as the number of galaxies we have in the signal detection. We found that the variance of the shear is still negligible with respect to the signal. The mean number of galaxies in the signal detection depends on the smoothing scale: larger the smoothing scale, larger the number of galaxies per window. We then have to check that for each smoothing scale (i.e. each number of galaxies per window) the variance of the shear measured in the catalogues where galaxies are sorted according to the star anisotropy, the optical distortion, or to the CCD frame, is negligible compared to the variance of the shear measured on the galaxy catalogues using the spatial averaging

Figure 7 shows that this is indeed the case. The three panels from top to bottom show respectively the star anisotropy case, the optical distortion case and the CCD frame case. On each panel, the thick solid line is the signal with its error bars derived from 1000 randomizations. The short dashed lines show the $\pm 1\sigma$ of these error bars centered on zero. On the top panel the two thin solid lines show $\langle \gamma^2 \rangle$ respectively measured with the galaxies sorted according to $e_1^{\rm stars}$ and to $e_2^{\rm stars}$. The thin solid line on middle panel shows $\langle \gamma_t^2 \rangle$ measured from the galaxies sorted according to their distance from the optical center, and the two thin solid lines in the bottom panel show $\langle \gamma^2 \rangle$ measured on the galaxies sorted according to X and Y.

In all the cases, the thin solid lines are consistent with the $\pm 1\sigma$ fluctuation, without showing a significant tendency for a positive $\langle \gamma^2 \rangle$. We conclude that the residual systematics are unable to explain the measured $\langle \gamma^2 \rangle$ in our survey, and unless we forgot an unknown systematic, our signal is likely to be of cosmological origin.

A direct test of the cosmological origin is to measure the correlation functions $\langle e_t(0) e_t(\theta) \rangle$, $\langle e_r(0) e_r(\theta) \rangle$

the radial component of the shear respectively:

$$e_t = -e_1 \cos(2\theta_k) - e_2 \sin(2\theta_k)$$
$$e_r = -e_2 \cos(2\theta_k) + e_1 \sin(2\theta_k), \quad (16)$$

where θ_k is the position angle of a galaxy. If the signal is of cosmological origin, we can show (Kaiser 1992) that $\langle e_t(0)e_t(\theta)\rangle$ should be positive, $\langle e_r(0)e_r(\theta)\rangle$ should show a sign inversion at intermediate scales, and $\langle e_r(0)e_t(\theta)\rangle$ should be zero. This is the consequence of the scalar origin of the gravitational lensing effect and of the fact that galaxy ellipticity components are uncorrelated. Although we do not have yet enough data to perform an accurate measure of these correlation functions, and to do any scientific analysis of them, it is interesting to check the general behavior of the correlation functions. Figure 8 shows that in our data set, although the measurement is very noisy, both $\langle e_t(0)e_t(\theta)\rangle$ and $\langle e_r(0)e_r(\theta)\rangle$ are positive valued, while $\langle e_r(0)e_t(\theta)\rangle$ is consistent with zero. This measurement demonstrates that the component of the galaxy ellipticities e_α of well separated galaxies are uncorrelated, and it is in some sense a strong proof that our signal at small scale is of cosmological origin, since only a lensing effect is likely to produce such behaviors.

The last thing we have checked is the stability of the results with respect to the field selection. We verified that removing one of the fields consecutively for all the fields (see Section 2 for the list of the fields) does not change the amplitude and the shape of the signal. This ensures that the signal is not produced by one field only, and that they are all equivalents in terms of image quality, PSF correction accuracy and signal amplitude, even using V and I colors. It also validates the different pre-reduction methods used for the different fields.

6. Cosmological constraints

Figure 1 provides a first comparison of our signal with some cosmological models. However, if we want to rule out models we need to estimate first the cosmic variance of the variance of the shear. Although it has not been yet exactly derived analytically (because the calculations in the non-linear regime are tricky), ray-tracing simulations can give a good estimate of it. We used the ray-tracing simulations of Jain et al. 1999 for this purpose.

Table 2 shows the two simulations we used. The τCDM model with $\sigma_8 = 1$ is not an independent simulation, but was constructed from the τCDM model with $\sigma_8 = 0.6$ simply by dividing κ by 0.6. This should empirically mimic a model with both Ω_0 and σ_8 equal to one. The redshift of the sources is equal to 1, which is certainly not fully appropriate for our data, however, according to the depth of the survey, we believe that it represents fairly the mean redshift of the galaxies. Figure 9 shows the amplitude and

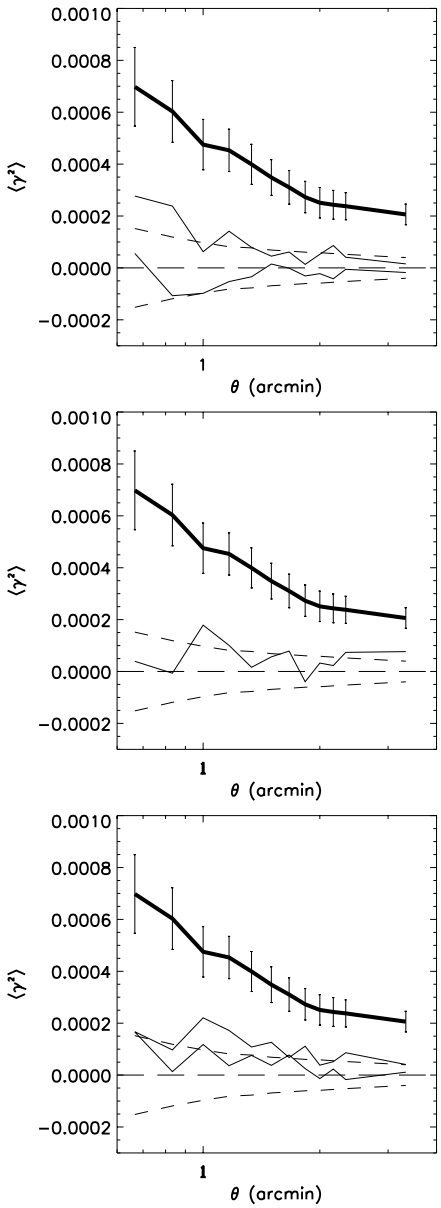

Fig. 7. Possible contribution of the systematics studied in Section 3.2 to the signal. On each of the plots, the thick solid line shows the signal as displayed on Figure 1, and the dashed lines show the $\pm 1\sigma$ fluctuation obtained from 1000 random realizations. From top to bottom: (a) The two thin solid lines are $\langle\gamma^2\rangle^{1/2}$ measured on the galaxies sorted according to the star ellipticity strength (see Figure 4). For the different smoothing scales, the mean number and the variance of the number of galaxies in the chosen bins fit the one observed in the signal (thick solid) curve. (b) the thin solid line is $\langle\gamma_t^2\rangle^{1/2}$ measured on the galaxies sorted according to the distance from the optical center, and on (c) the two thin solid lines correspond to the galaxies are sorted according to their X or Y location on the CCDs.

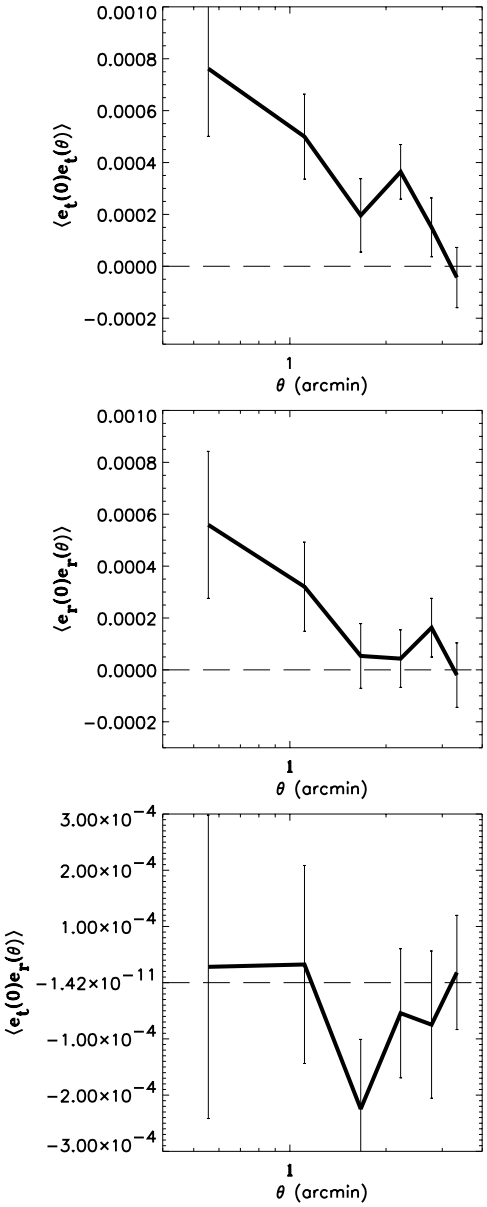

Fig. 8. From top to bottom, measurement of the correlation functions $\langle e_t(0)e_t(\theta)\rangle$, $\langle e_r(0)e_r(\theta)\rangle$ and $\langle e_r(0)e_t(\theta)\rangle$. The error bars are computed from a 50 random realizations of our data set where the orientation of the galaxies were randomized.

Table 2. List of the ray tracing simulations we used (see Jain et al. 1999 for details). The redshift of the sources is 1.

Simulation #	Γ	Ω_0	Λ	σ_8
(1) OCDM	0.21	0.3	0	0.85
(2) τCDM	0.21	1	0	0.6
(3) τCDM	0.21	1	0	1

three cosmological models, compared to our signal. It is remarkable that models (1) and (3) can be marginally rejected (We did not plot the error bars due to the intrinsic ellipticity for clarity: they can be read from Figure 7). The data are in agreement with the cluster normalized model (2). Also plotted is the theoretical prediction of a ΛCDM model, with $\Omega = 0.3$, $\Lambda = 0.7$, $\Gamma = 0.5$ and a redshift of the sources $z_s = 1$. It shows that low-Ω model is also in perfect agreement with the data, which means that weak gravitational lensing provides cosmological constraints similar to the cluster abundance tests (Eke et al. 1996): the second moment of the shear measures a combination of σ_8 and Ω_0 (see equation 8). A measure of the third moment of the convergence would break the Ω-σ_8 this degeneracy, but this requires more data (see Bernardeau et al. 1997, Van Waerbeke et al. 1999). It should also be noted that for the simulations, we have considered cold dark matter models with shape parameter $\Gamma = 0.21$; higher values of Γ increases the theoretical predictions, e.g. the $\Omega_0 = 1$, $\sigma_8 = 1$ would be ruled out even more strongly. We conclude that our analysis is consistent with the current favored cosmological models, although we cannot yet reject the other models with high significance. Since we only analyzed 2 square degrees of the survey, with forthcoming larger surveys we should be able to set strong constraints on the cosmological models as discussed below.

We should emphasize that due to the imprecise knowledge of the redshift distribution in our data, the prediction might still be subject to modifications. The final state of our survey in 4 colors will however permits the measurement of this distribution.

7. Conclusion

We have demonstrated the existence of a significant correlation between galaxy ellipticities from 0.5 to 3.5 arcminutes scales. The signal has the amplitude and the angular dependence expected from theoretical predictions of weak lensing produced by large-scale structures of the universe. We have tested the possible contribution of systematic errors to the measured signal; in particular we discussed three potential sources of spurious alignment of galaxies: overlapping isophotes of very close galaxies, star anisotropy and CCD line/column alignment. The first of these systematics is easy to deal with, simply by removing close pairs, although we may have decreased the signal slightly by removing them. The star anisotropy seems to be very well controlled, in part due to the fact that the bias adds quadratically with the signal. Moreover, in the absolute sense, the bias does not exceed a fraction of 1 percent, which is adequate to accurately measure a variance of the shear of few percent. The only important bias we found seems to be associated with the CCD columns, and it is constant over the survey, it is therefore easy to correct for. The origin of this CCD bias is still unclear.

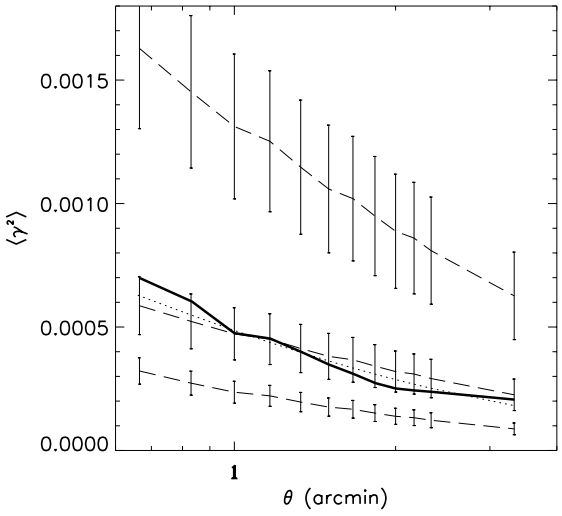

Fig. 9. Comparison of our signal (thick line) with three cosmological models. The error bars are the cosmic variance measured on five independent realizations at the smoothing scale indicated by the x-axis. For clarity, the shot noise error bars of the signal are not plotted, their amplitude can be read on Figure 7. From bottom to top, the dashed lines correspond to: model (1), model (2) and model (3) as given in Table 2. The shot-noise error bars of the signal are in fact comparable in amplitude to the cosmic variance error bars of model (2). We show also a cluster-normalised Λ model (dotted line) with $\Omega = 0.3$, $\Lambda = 0.7$, and a CDM power spectrum with $\Gamma = 0.5$. This model was not obtained from a simulation, but computed using the non-linear power spectrum using the Peacock & Dodds 1996 formula.

As an objective test of the reality of the gravitational shear signal, we measured the ellipticity correlation functions $\langle e_t(0)e_t(\theta)\rangle$, $\langle e_r(0)e_r(\theta)\rangle$ and $\langle e_r(0)e_t(\theta)\rangle$. While the measurement is noisy, the general behavior is fully consistent with the lensing origin of the signal. The tests for systematic errors and the three ellipticity correlation function measurements described above have led us to conclude with confidence that we have measured a cosmic shear signal.

With larger survey area, we expect to be able to measure other lensing statistics, like the aperture mass statistic ($M_{\rm ap}$; see Schneider et al. 1998). The $M_{\rm ap}$ statistic is still very noisy for our survey size because its signal-to-noise is much lower than the top-hat smoothing statistic, due to higher sample variance (We verified this statement using the ray tracing simulation data of Jain et al. 1999). Our survey will increase in size in the near future (quickly up to 7 square degrees), leading to a factor of 2 improvement in the signal-to-noise of the results presented here. According to our estimates, this will be enough to measure $M_{\rm ap}$ at the arcminute scale with a signal-to-noise of $\sim$ 3. The detection of the skewness of the convergence should also be possible with the increased generacy between the amplitude of the power spectrum and Ω. These measures should also provide nearly independent confirmations of the weak gravitational lensing effect as well as additional constraints on cosmology. Thus by combining different measures of lensing by large-scale structure (top-hat smoothing statistics, $M_{\rm ap}$ statistics, correlation function analysis, power spectrum measurements), higher order moments, and peak statistics (Jain & Van Waerbeke 2000), from forthcoming survey data, we hope to make significant progress in measuring dark matter clustering and cosmological parameters with weak lensing.

We do not hope to do a much broader analysis (than the variance of the shear, the shear correlation function, and possibly the skewness of κ) with the actual *state of art* PSF correction quality. For instance mass reconstruction is linear with the amplitude of the residual bias, and a fraction of percent bias is still high enough to prevent definitive filaments detection or to map the details of large scale structures. Since we show elsewhere (Erben et al. 2000) that such bias is unavoidable with the present day correction techniques and image quality, there is still to improve the analysis prior to get accurate large-scale mass maps. However we hope to be on the right direction and some very recent huge effort to improve the PSF correction is very encouraging (Kaiser 1999). We plan to go toward these further steps once we will get a more homogeneous data set on a much larger field.

Acknowledgements. T. Erben and R. Maoli thank CITA for hospitality, L. Van Waerbeke thanks IAP and MPA for hospitality, F. Bernardeau, J.-C. Cuillandre and T. Erben thank IAP for hospitality. We thank M. Crézé and A. Robin for providing their UH8K data of SA57. We thank P. Couturier for the allocation of CFHT discretionnary time to observe the Abell 1942 cluster with UH8K. This work was supported by the TMR Network "Gravitational Lensing: New Constraints on Cosmology and the Distribution of Dark Matter" of the EC under contract No. ERBFMRX-CT97-0172, and a PROCOPE grant No. 9723878 by the DAAD and the A.P.A.P.E. We thank the TERAPIX data center for providing its facilities for the data reduction of the CFH12K and UH8K data.

References

Annis, J., Frieman, J., Joffre, M., Johnstone, D., McKay T., Nichol, B., Stebbins, A., 1998. In *Wide Field Surveys in Cosmology.* S. Colombi, Y. Mellier, B. Raban eds. Frontières

Bartelmann, M., Schneider, P., 1999, A& A, 345, 17

Bartelmann, M., Schneider, P. 1999, astro-ph/9912508

Bertin, E., in preparation

Bertin, E., Arnouts, S., 1996, A& A, 117, 393

Bernardeau, F., Van Waerbeke, L., Mellier, Y., 1997, A& A, 322, 1

Bonnet, H., MellierY., 1995, A& A, 303, 331

Murowinski, R., Crampton, D., Wooff, R., Luppino, G. A. 1996. PASP 108, 1120
Cuillandre, J.-C., Luppino, G., Starr, B., Isani, S. 2000. In *Optical Detectors for Astronomy*. P. Amico, J.W. Beletic eds. ASSL Series. Kluwer 2000.
Eke, V.R., Cole, S., Frenk, C.S, 1996, MNRAS, 282, 263
Erben, T., et al. in preparation
Hoekstra, H., Franx, M., Kuijken, K., Squires, G., 1998, ApJ, 504, 636
Jain, B., Seljak, U., 1997, ApJ, 484, 560
Jain, B., Seljak, U., White, S., ApJ, in press, astro-ph/9901287
Jain, B., Van Waerbeke, L., 2000, ApJL, 530, L1
Kaiser, N., 1992, ApJ, 388, 272
Kaiser, N., 1998, ApJ, 498, 26
Kaiser, N., 1999, ApJ, submitted, astro-ph/9904003
Kaiser, N., Squires, G., Broadhurst, T., 1995, ApJ, 449, 460
Kaiser, N., Wilson, G., Luppino, G., Kofman, L., Gioia, I., Metzger, M., Dahle, H., ApJ submitted, astro-ph/9809268
Kuijken, K., 1999, A& A, 352, 355
Le Fèvre, O., Vettolani, G., Maccagni, D., Mancini, D., Picat, J.-P., Mellier, Y., Mazure, A., Arnaboldi, M., Charlot, S., Cuby, J.-G., Guzzo, L., Scaramella, R., tresse, L., Zamorani, G., 1998. In *Wide Field Surveys in Cosmology*. S. Colombi, Y. Mellier, B. Raban eds. Frontières
Luppino, G., Bredthauer, R., Geary, J. C., 1994, SPIE 2198, 810
Luppino, G., Kaiser, N., 1997, ApJ, 475, 20L
Mellier, Y., 1999, ARAA, 37, 127
Peacock, J.A., Dodds, S.J., 1996, MNRAS, 280, L9
Rhodes, J., Refregier, A., Groth, E., ApJ submitted, astro-ph/9905090
Schneider, P., Van Waerbeke, L., Jain, B., Kruse, G., 1998, MNRAS, 296, 873S
Seitz, S., Collodel, L., Pirzkal, N., Erben, T., Freudling, W., Schneider, P., Fosbury, B., White, S. D. M. 1998. In *Wide Field Surveys in Cosmology*. S. Colombi, Y. Mellier, B. Raban eds. Frontières
Van Waerbeke, L., Mellier, Y., Schneider, P., Fort, B., Mathez, G, 1997, A& A, 317, 303
Van Waerbeke, L., Bernardeau, F., Mellier, Y., 1999, A& A, 342, 15
Villumsen, J., 1996, MNRAS, 281, 369

This article was processed by the author using Springer-Verlag LaTeX A&A style file *L-AA* version 3.

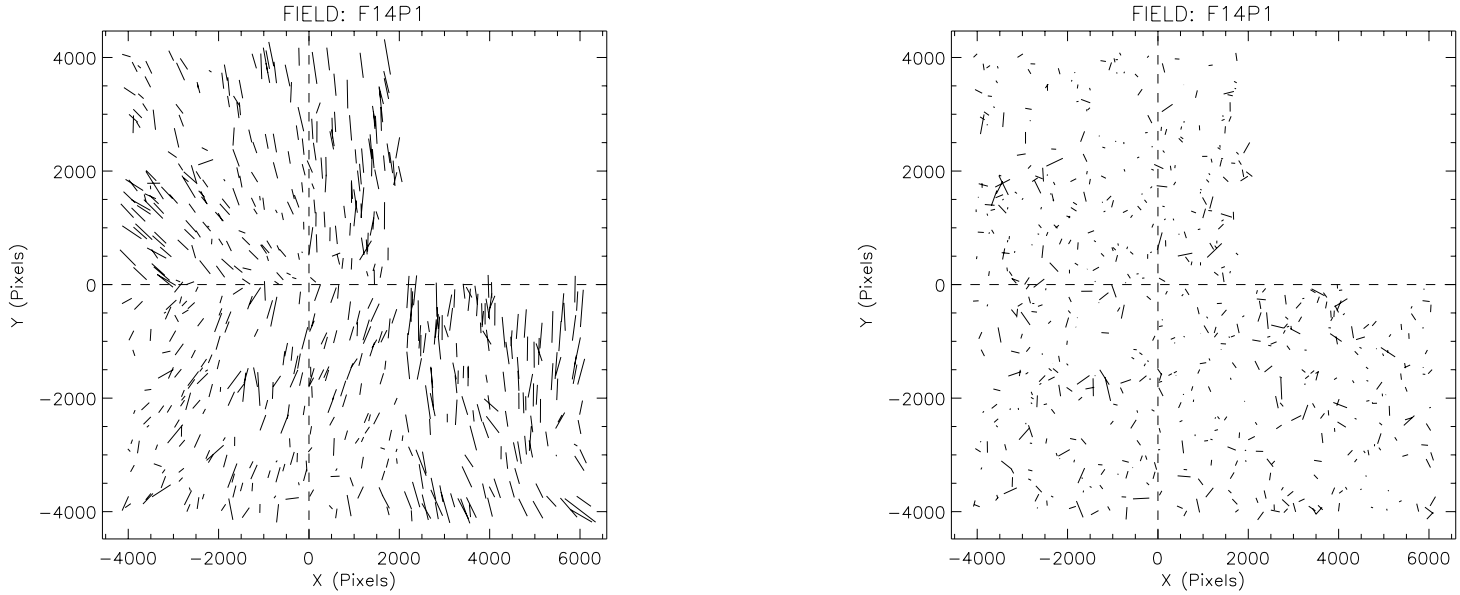

Fig. 10. Uncorrected (left) and corrected (right) star ellipticities for FIELD F14P1. The dashed cross shows the location of the optical center. Frames are graduated in pixels.

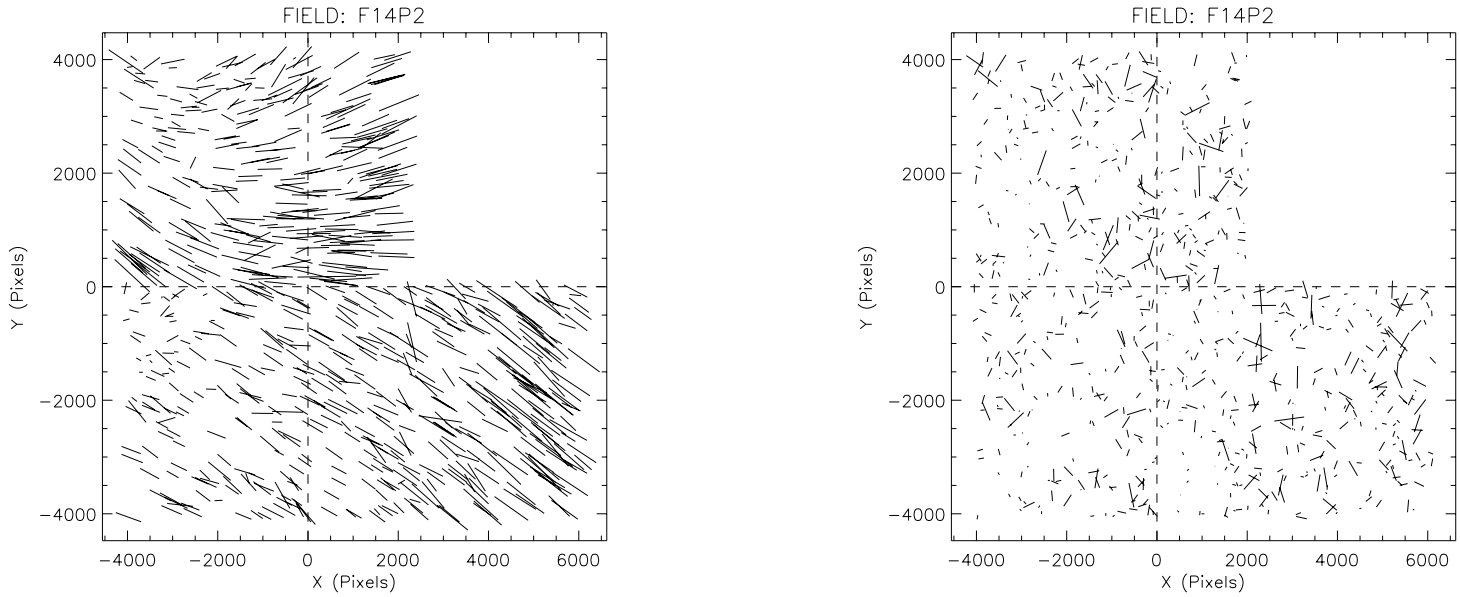

Fig. 11. Same as Figure 10 for FIELD F14P2.

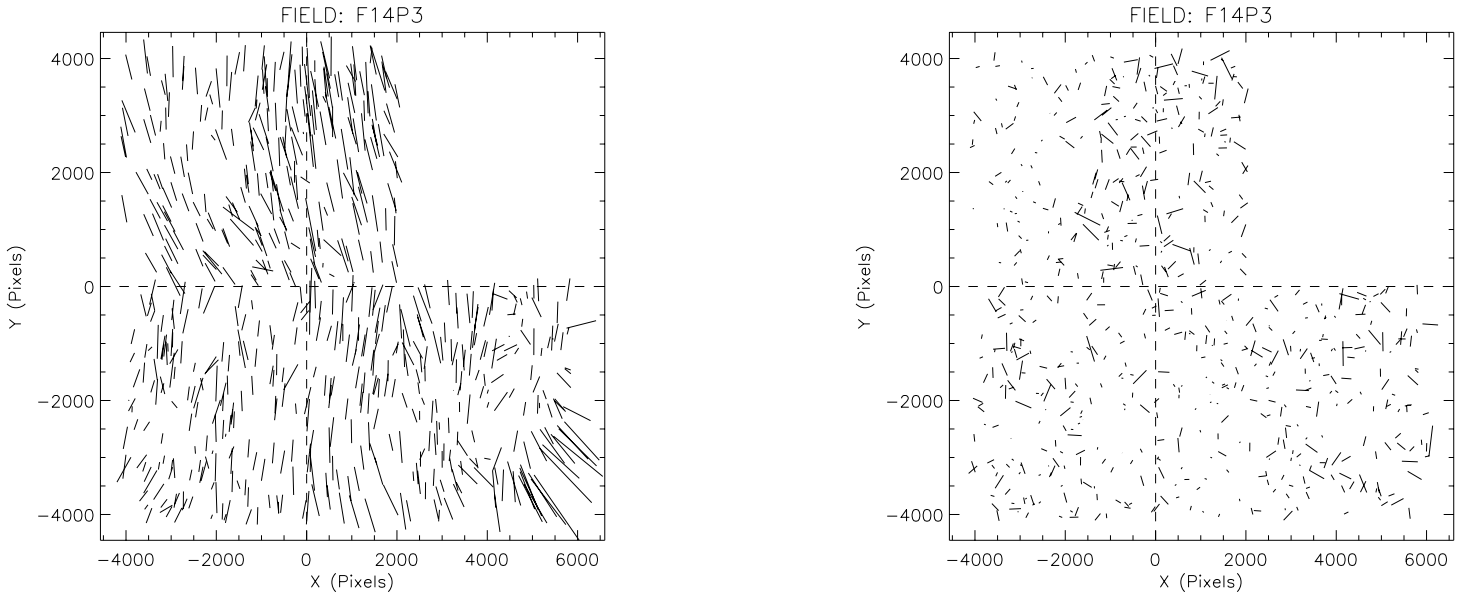

Fig. 12. Same as Figure 10 for FIELD F14P3.

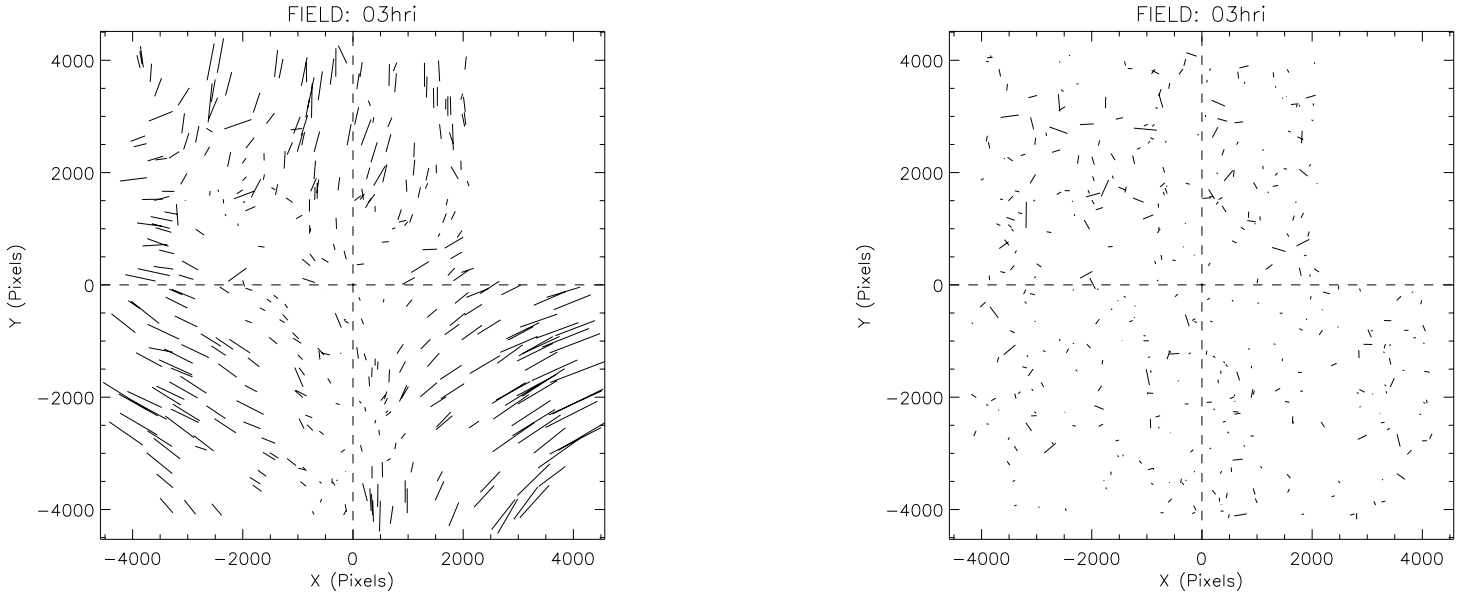

Fig. 13. Same as Figure 10 for FIELD 03hrie.

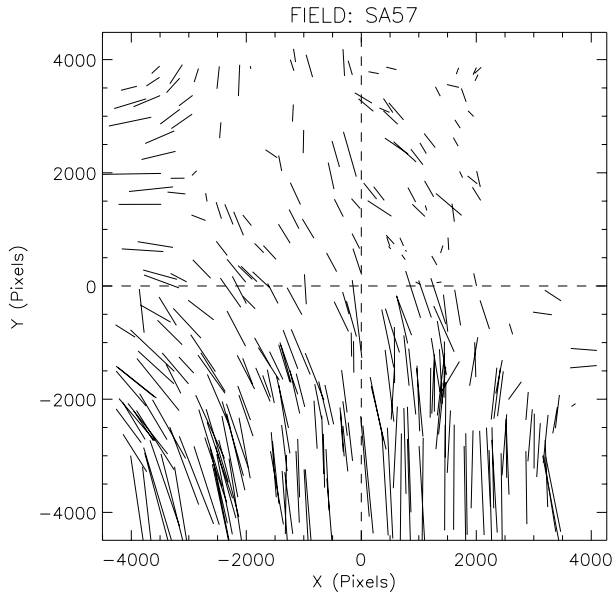

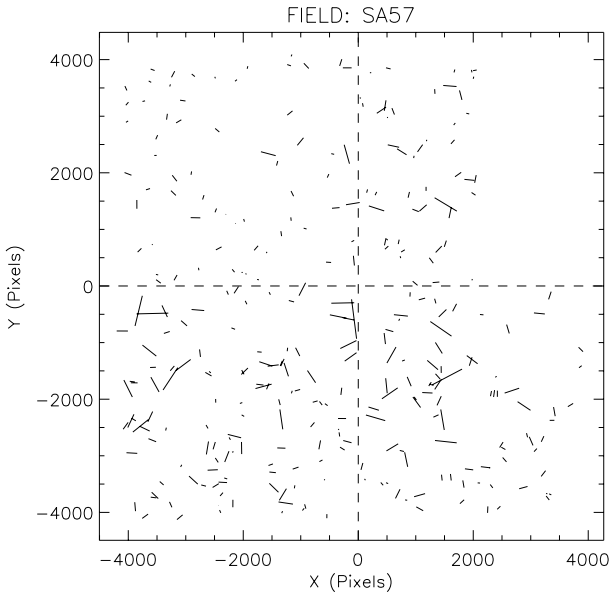

Fig. 14. Same as Figure 10 for FIELD SA57.

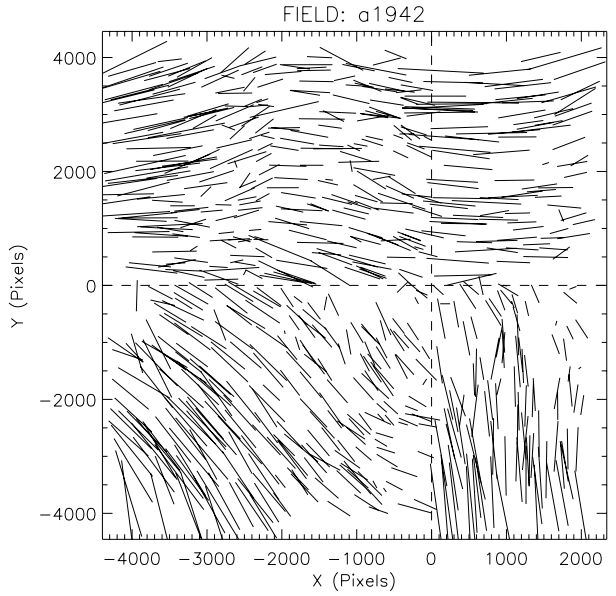

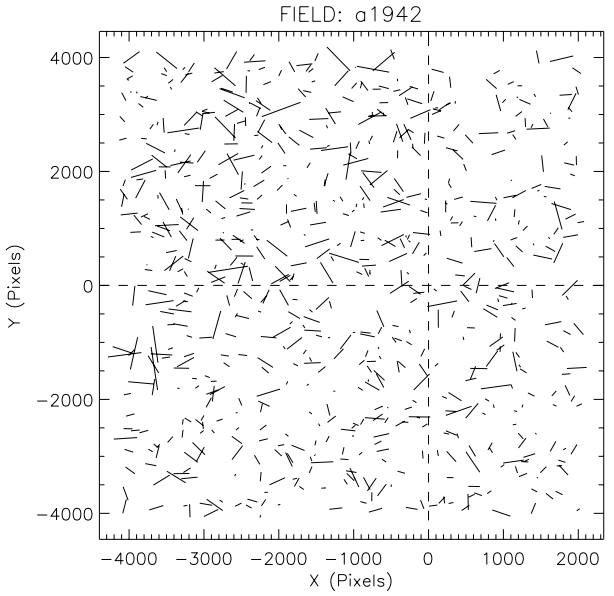

Fig. 15. Same as Figure 10 for FIELD a1942.

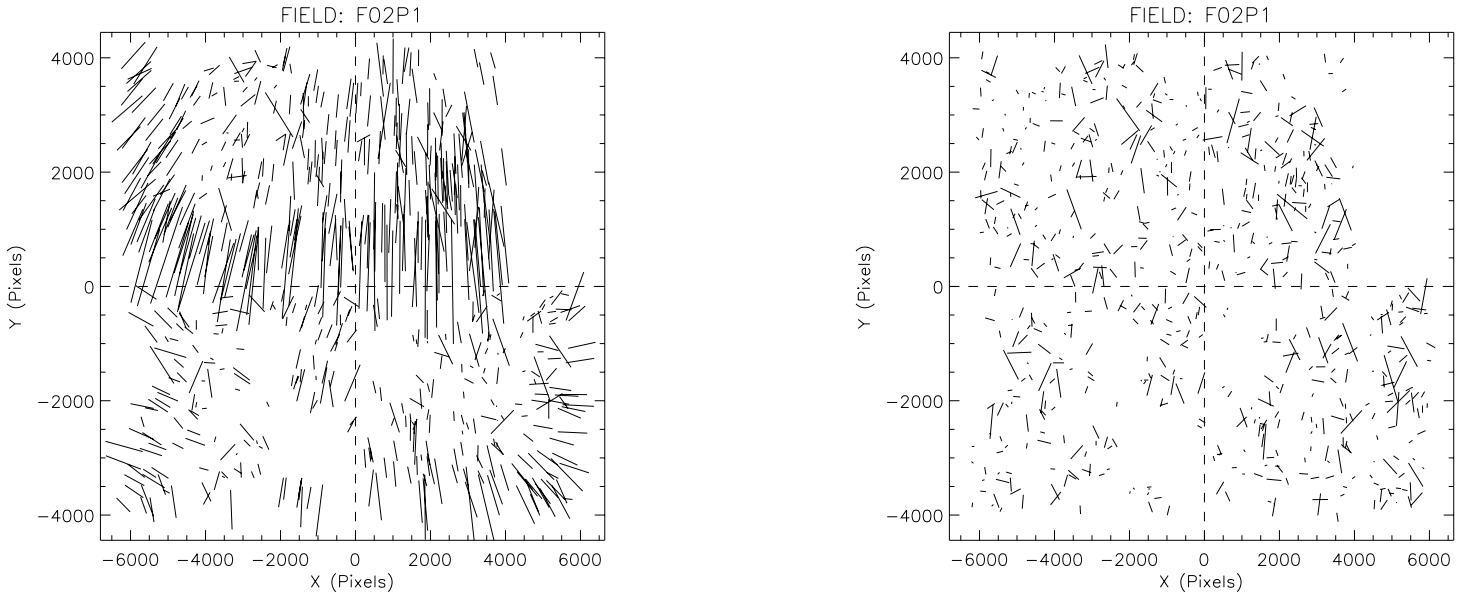

Fig. 16. Same as Figure 10 for FIELD F02P1.

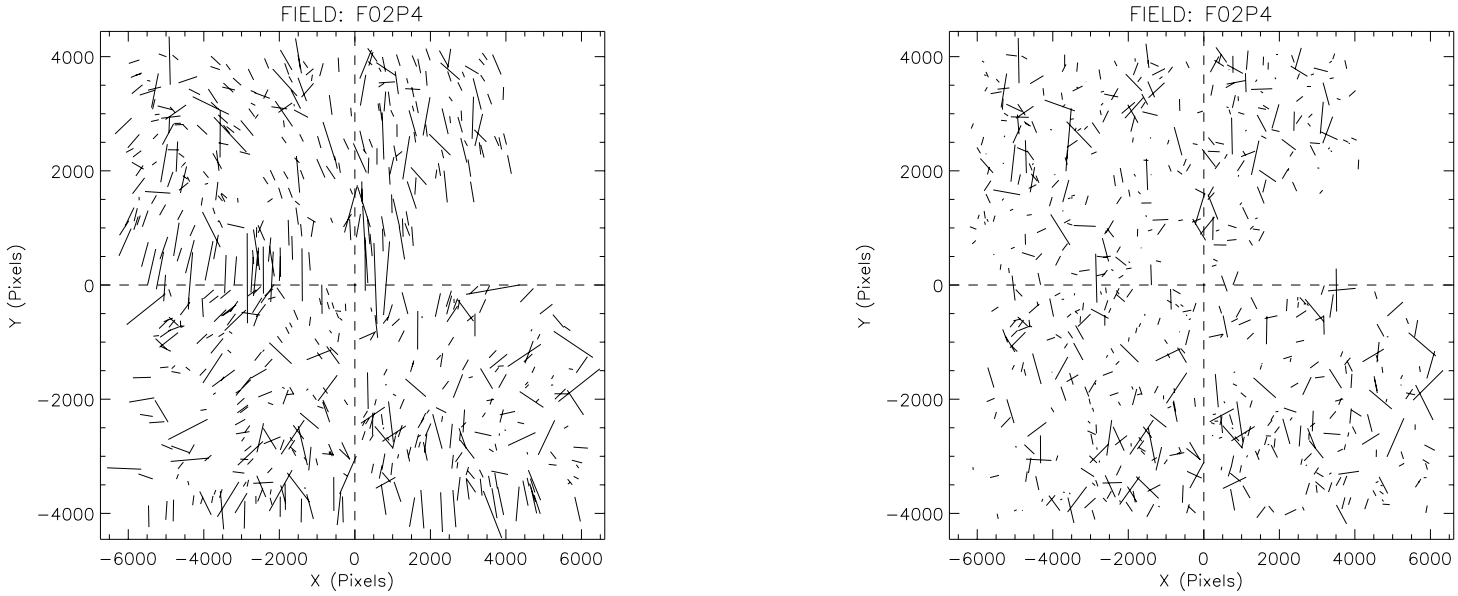

Fig. 17. Same as Figure 10 for FIELD F02P4.